Journal of Structural Geology, Vol. 12, No. 4, pp. 483 to 498, 1990
Printed in Great Britain

0191-8141/90 $03.00+0.00
Pergamon Press plc

Orientation history and rheology in slates, Kodiak and Afognak Islands, Alaska

DONALD M. FISHER*

Department of Geological Sciences, Brown University, Providence, RI 02912, U.S.A.

(*Received* 26 *July* 1989; *accepted in revised form* 30 *December* 1989)

Abstract—Theoretical and experimental studies have shown that slates have a roughly parabolic yield curve in $\phi - \sigma$ and $\Phi - \sigma$ space, where ϕ is the orientation of cleavage relative to the maximum compressive stress, Φ is the orientation of cleavage relative to the incremental shortening direction and σ is the deviatoric stress. Deformation mechanisms that operate in low-grade rocks such as diffusive mass transfer in a grain boundary fluid, dislocation creep and frictional grain boundary sliding may have stress–strain rate relationships that depend on ϕ. During a progressive strain history, ϕ and Φ may vary as a function of the strain path. Thus, the sequence of dominant deformation mechanisms as well as the stress–strain history may depend on the orientation history or variations in Φ as strain accumulates.

In the Kodiak Formation, a slate belt in southwest Alaska, the orientation history and deformation mechanisms were evaluated using incremental strain indicators and microstructures. There are four successive textural events: (1) development of a slaty cleavage (S_2) with antitaxial growth of fibrous quartz and mica in pressure shadows (Fi_2); (2) static growth of siderite and chlorite porphyroblasts; (3) 10–70° rotation of porphyroblasts relative to S_2 with growth of curved syntaxial siderite fibers; and (4) antitaxial growth of fibrous quartz and micas with local development of a crenulation cleavage (S_3). Cumulative incremental strain and progressive finite strain histories were determined in 23 samples from syntectonic fibers, and orientation histories were reconstructed from information provided by cumulative incremental strain histories. Textural and strain analyses indicate that: (1) the strain history of nearly all samples can be approximated by two coaxial strain accumulations separated by a rigid rotation; (2) development of crenulation cleavages was dependent on the orientation history and the magnitude of the early strain accumulation (i.e. the degree of mica alignment at the completion of D_2); (3) unstable behavior, or buckling, occurred when $\Phi < 45°$, suggesting that the angle of internal friction (Ψ) was close to 0° (i.e. basal slip in micas may have been more important than frictional grain boundary sliding); and (4) diffusive mass transfer was accompanied by anisotropic plastic deformation, so the orientation history could be used to reconstruct the $\sigma - \varepsilon$ history.

INTRODUCTION

SPATIAL variations in the relationship between stress and strain determine the structural morphology of an orogenic belt. In both extensional and compressional regimes, a large portion of the strain can be localized in shear zones (Ramsay & Graham 1970). Strain localization requires that the rocks within the shear zone experience strain softening (Cobbold 1977, White *et al.* 1980), so that the flow stress within the shear zone is lower than the yield stress of the material outside the zone. In contrast, strain hardening can cause deformation to be progressively dispersed over a wider area. Strain softening and strain hardening rheologies reflect grain scale deformation processes that respond to variables such as grain size, temperature and fluid pressure. In this paper, I consider the effect of thc orientation history on the rheology and microstructural evolution of foliated rocks.

Theoretical (Cobbold 1977, Reches 1979) and experimental (Donath 1961, 1964, 1968, Patterson & Weiss 1966) studies have attempted to characterize the rheology of foliated rocks. For a plastic material, the stress–strain behavior can be described by the strength, or yield stress, of the material. Donath (1961, 1964) demonstrated experimentally that the strength of Martinsburg slate depends on the orientation of the cleavage relative to the incremental shortening direction (the axis of deformed cores, or ε_3). When the cleavage is either parallel or perpendicular to ε_3, there is no resolved shear stress on the anisotropy, and the yield stress is maximized. When the cleavage is inclined relative to ε_3, the yield stress is smaller. This relationship can be characterized by a roughly parabolic yield curve in $\Phi - \sigma$ space, where Φ is the orientation of the cleavage with respect to ε_3, and σ is the deviatoric stress (Fig. 1) (Donath 1961, 1964).

Reches (1979) derived a parabolic yield curve for a foliated plastic material. The orientation of the anisotropy was described with respect to σ_1. In an anisotropic material, the orientation of incremental shortening may not be parallel to σ_1. Because the triaxial experiments of Donath (1961, 1964, 1968) constrain the axis of shortening and not the precise orientation of σ_1 within the material, the general agreement between the work of Reches (1979) and the experiments of Donath (1961, 1964) suggest that the difference in orientation between σ_1 and ε_3 is not large; thus, shear failure of slates can be described by a roughly parabolic yield curve, regardless of whether the orientation of the foliation is described relative to σ_1 or ε_3.

Reches (1979) used the parabolic yield curve to describe the rheology of foliated rocks. During a coaxial strain history, the stress–strain relationship depends on the initial orientation of the cleavage relative to σ_1, or

*Present address: Department of Geosciences, Pennsylvania State University, University Park, PA 16802, U.S.A.

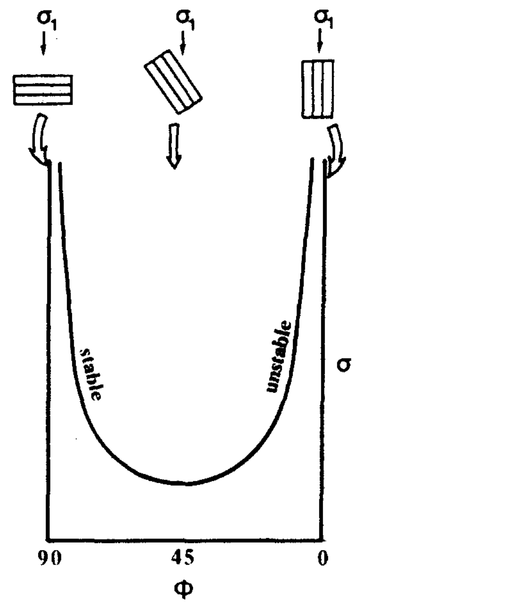

Fig. 1. Parabolic yield curve for slates, where ϕ is orientation of slaty cleavage relative to maximum compressive stress (σ_1) and σ is deviatoric stress. Yield curve is drawn for case where angle of internal friction (Ψ) = 0°.

ϕ_0. Deformation occurs when the deviatoric stress equals the yield strength for the initial orientation, but, given a finite strain accumulation, the value of ϕ approaches 90°. If the cleavage has an initial orientation of between 0° and $(45° - \Psi/2)°$ (where Ψ is the angle of internal friction), strain occurs at a progressively lower deviatoric stress, and slip on cleavage is unstable (Fig. 1) (Reches 1979). Unstable slip is accompanied by buckling of the anisotropy. Alternatively, if the cleavage has an initial orientation between $(45 - \Psi/2)°$ and 90°, additional strain increments require a greater deviatoric stress (e.g. strain hardening) and slip on cleavage is stable (Fig. 1) (Reches 1979).

Recently, it has become apparent that strain paths in slates are typically non-coaxial, with complex incremental strain histories that depend on position within thrust sheets, the geometry of thrust fault surfaces (Butler 1982, Sample & Fisher 1986, Beutner *et al.* 1988), position with respect to folds (Wickham & Anthony, 1977, Beutner & Diegel 1985, Tapp & Wickham 1987) and the kinematics of folding (Beutner & Diegel 1985). Under these circumstances, Φ, the orientation of the cleavage relative to the incremental shortening direction, varies as a function of the strain path.

The goals of this paper are: (1) to consider the relationship between deformation mechanisms, strain path and stress–strain history in slates at low-grade conditions; and (2) to apply this relationship to the Kodiak Formation, a slate belt exposed on Kodiak and Afognak Island, Alaska, where a variety of incremental strain indicators can be combined with a detailed textural history.

DEFORMATION MECHANISMS IN SLATES

At lower greenschist-facies conditions and geologically reasonable strain rates, frictional sliding and cataclasis, as described in the room temperature experiments of Donath (1961, 1964) and Patterson & Weiss (1966), are not the only possible deformation mechanisms in slates. One important deformation mechanism in low-grade metamorphic rocks is diffusive mass transfer in a grain boundary fluid. This mechanism is accompanied by relative grain motions and could be described as diffusion accommodated particulate flow (Elliott 1973). Diffusive mass transfer can be either diffusion controlled (Berner 1978), whereby the rate-controlling step is the diffusion of species from the site of dissolution to the site of precipitation, or interface controlled (Berner 1978), whereby the rate-controlling step is the dissolution and/or precipitation of material. In the case of interface controlled diffusive mass transfer, crystallographic control on the rate of dissolution/precipitation of micas could result in a ϕ dependence. Because the flow law for diffusive mass transfer involves a linear relationship between stress and strain rate (Elliott 1973), a dependence on ϕ could be represented by anisotropic viscous behavior (Lipshitz 1963).

Other ϕ-dependent deformation mechanisms in slates may result in plastic behavior. For example, deformation may occur by dislocation creep in micas with slip favored along the basal planes (Kronenberg *et al.* 1985). Alternatively, deformation may be accomplished by independent particulate flow, with frictional slip along grain boundaries (Borradaile 1979). Particulate flow is favored by high pore fluid pressures (Borradaile 1981), a condition that may be characteristic of slates and other regionally metamorphosed rocks (Etheridge *et al.* 1983). Because the foliation in pelitic rocks can be defined by the preferred alignment of both grain boundaries and basal planes in fine-grained micas, plastic deformation by either of these mechanisms may be characterized by a parabolic yield curve. When deformation occurs by dislocation creep in micas, the angle of internal friction (Ψ) may be close to 0°, and the field of unstable behavior may encompass all ϕ values from 0° to 45°. When deformation occurs by frictional grain boundary sliding, Ψ may be close to 30°, and the field of unstable behavior is smaller.

Diffusive mass transfer, independent particulate flow and dislocation creep are independent mechanisms, and the dominant mechanism produces the greatest portion of the bulk strain rate. When an increasing deviatoric stress is applied, a rock will deform by diffusive mass transfer at an increasing strain rate until the yield stress for plastic processes is attained. During subsequent increases in bulk strain rate, the strain rate produced by diffusive mass transfer and the flow stress within the material will remain constant, but dislocation creep and/or independent particulate flow will occur at a greater rate. Thus, increases in bulk strain rate can lead to a dominance of plastic deformation mechanisms. In slates, diffusive mass transfer would be the only operative mechanism if the applied stress were lower than the yield stress for plastic processes at a given ϕ value.

Consider the case where diffusive mass transfer is not dependent on ϕ (μ, the viscosity, is not a function of ϕ).

As ϕ approaches 45 − $\Psi/2°$, the yield stress for plastic processes (dislocation creep or frictional sliding of micas) decreases. Consequently, the strain rate contributed by diffusive mass transfer in a grain boundary fluid would be smaller, and plastic processes dominate at a smaller bulk strain rate. Alternatively, as ϕ approaches 90°, the yield stress for plastic processes is greater, and the bulk strain rate at which plastic processes dominate is also greater. Thus, given a constant bulk strain rate, the dominant deformation mechanism may be a function of ϕ, and the sequence of dominant deformation mechanisms during a progressive strain history depends on the orientation history, or variations in the value of Φ as strain accumulates.

ORIENTATION HISTORIES IN SLATES

The orientation history of a rock with a strong foliation, either sedimentary layering or a tectonic cleavage, can be represented on an orientation history diagram, with the orientation of incremental shortening relative to the foliation (Φ) as the x axis and the cumulative incremental strain (ε) as the y axis (Fig. 2).

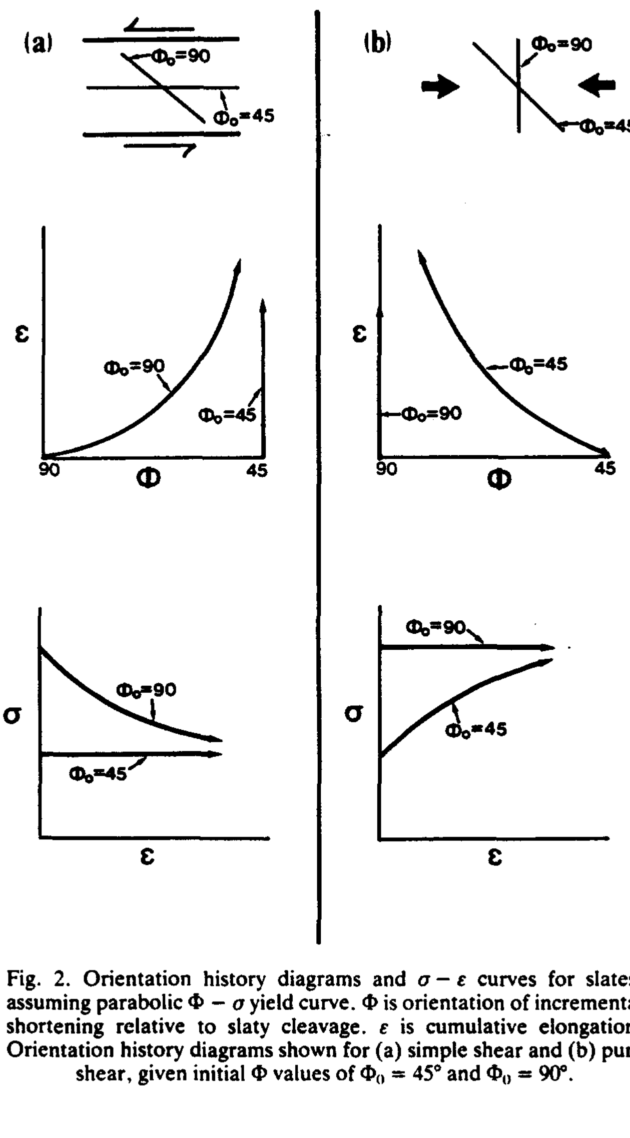

Fig. 2. Orientation history diagrams and $\sigma - \varepsilon$ curves for slates, assuming parabolic $\Phi - \sigma$ yield curve. Φ is orientation of incremental shortening relative to slaty cleavage. ε is cumulative elongation. Orientation history diagrams shown for (a) simple shear and (b) pure shear, given initial Φ values of $\Phi_0 = 45°$ and $\Phi_0 = 90°$.

The rheology of foliated rocks depends on both the initial orientation (Φ_0) and the orientation history. If Φ_0 is between 90° and 45 − $\Psi/2°$, simple shear can cause Φ to approach 45°. Thus, deformation occurs at a progressively lower stress and the contribution of plastic deformation mechanisms to a constant bulk strain rate will be larger. Simple shear in foliated rocks can result in geometric softening (White *et al.* 1980) or rotation softening (Cobbold 1977) which may lead to localization of shear strains in shear zones or at the base of thrust sheets. In contrast, coaxial flattening causes progressive rotation of the foliation towards the incremental extension direction, and the strain path asymptotically approaches $\Phi = 90°$. If Φ_0 is between 45 − $\Psi/2°$ and 90°, a coaxial strain path is a strain hardening path (Fig. 2). Given a constant bulk strain rate, coaxial flattening will result in an increase in the relative importance of diffusive mass transfer.

In foliated rocks, the orientation history can be determined using incremental strain indicators. Commonly used incremental strain indicators are syntectonic fibers in pyrite pressure shadows and veins. Fibers provide a record of changes in the incremental extension direction as strain accumulates, which can be used to evaluate the kinematics of folding (Wickham & Anthony 1977, Beutner & Diegel 1985, Tapp & Wickham 1987), cleavage development (Gray & Durney 1979) and thrust sheet deformation (Beutner *et al.* 1988). However, fibers may behave rigidly or deform passively (Ramsay & Huber 1983, Ellis 1986, Etchecopar & Malavieille 1987), so an assumption must be made about fiber behavior before fiber data from a pressure shadow can be translated into a $\Phi - \varepsilon$ path for the surrounding matrix.

Other useful incremental strain indicators in metamorphic rocks are syntectonic porphyroblasts (Elliott 1972). Porphyroblasts commonly include trails of a pre-existing foliation (S_i) that are rotated relative to the external fabric (S_e). When the difference in orientation between S_i and S_e is less than 90°, apparent rotations may be due to flattening and passive rotation of the foliation outside the porphyroblasts (Ramsay 1962, Kennan 1971, Bell *et al.* 1986) or to active rotation of the porphyroblasts in response to simple shear (Williams & Schoneveld 1981).

In the following sections, fibrous pressure shadows and syntectonic porphyroblasts from slates of the Kodiak Formation are used to characterize the sequence of deformation mechanisms and quantify the orientation history of these slates on a $\Phi - \varepsilon$ plot.

TEXTURAL HISTORY AND STRAIN PATH WITHIN THE KODIAK FORMATION

The early Maastrichtian Kodiak Formation is part of a slate belt that was accreted in the late Cretaceous or early Tertiary along the southwest Alaska convergent margin (Sample & Fisher 1986, Sample & Moore 1987), a margin that has been active since the late Cretaceous

(Moore *et al.* 1983, Byrne & Fisher 1987). The entire slate belt, which includes the Kodiak Formation, the Shumagin Formation, and the Valdez Group, continues parallel to the margin for over 1000 km (Fig. 3). In the Kodiak Islands, the Kodiak Formation strikes NE and encompasses over 60% of the Kodiak accretionary complex (Fig. 3).

The earliest deformation in the Kodiak Formation (D_1) is believed to have occurred during underthrusting and progressive lithification of a thick sediment pile (Fisher & Byrne 1987). This deformation resulted in the development of two distinct structural terranes; coherent terranes of layered turbidites and melange terranes. Within mélange terranes, D_1 is recorded in part by a pervasive scale foliation (S_1), with only local scaly microfractures within coherent terranes. The second deformation (D_2) resulted in the juxtaposition of accreted packages and the development of fold-and-thrust structures and an associated slaty cleavage (S_2). D_2 coincided with regional lower greenschist-facies metamorphism and preceded the intrusion of 60 Ma old plutons (Sample & Moore 1987). A third deformation (D_3) folded the accreted packages into a broad regional anticline that exposes the deepest D_2 structural levels in the core and progressively higher structural levels on either limb (Fig. 3). I will describe the microstructural evolution and strain history in samples from the upper structural levels of the Kodiak Formation (i.e. the landward (NW) and seaward (SE) limbs of the D_3 fold) and will focus on the effect of the orientation history on cleavage development and the associated mechanical behavior. A later paper (Fisher & Byrne in preparation) will address the regional significance of strain histories throughout the Kodiak Formation.

In the landward and seaward belts of the Kodiak Formation, the incremental strain histories associated

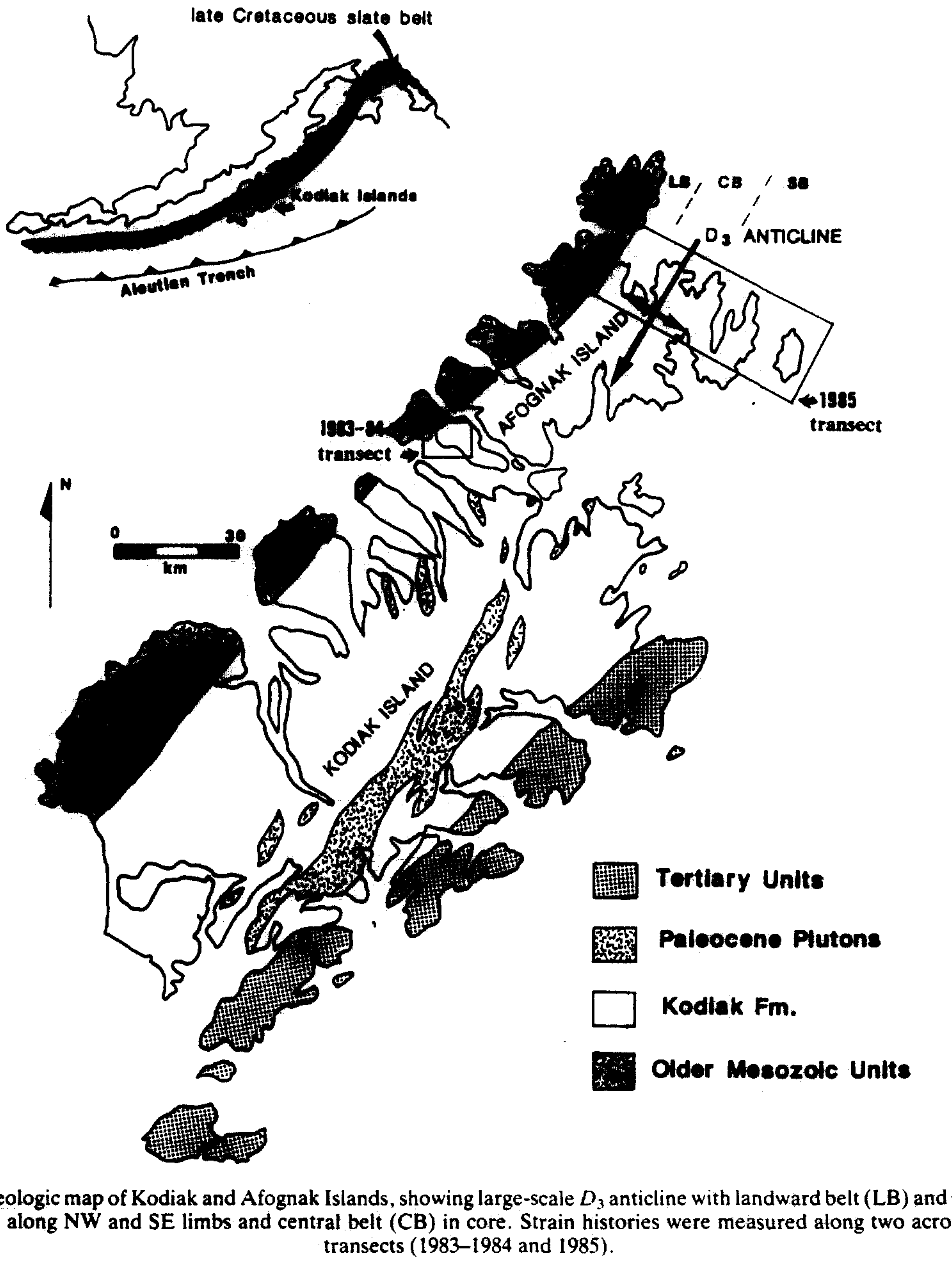

Fig. 3. Geologic map of Kodiak and Afognak Islands, showing large-scale D_3 anticline with landward belt (LB) and seaward belt (SB) along NW and SE limbs and central belt (CB) in core. Strain histories were measured along two across-strike transects (1983–1984 and 1985).

with both D_2 and D_3 microstructures were quantified using syntectonic fibers and porphyroblasts. The results of this strain analysis are described below.

Microstructures and incremental strain histories

D_2 deformation in the landward belt and seaward belt is marked by the development of a slaty cleavage (S_2), which strikes NE and dips steeply (45–90°) to the northwest. This cleavage is roughly axial planar to mesoscopic, SE-verging folds and is defined by the alignment of fine-grained chlorite and white mica grains and planar or anastomosing trails of opaque particles. The fine-grained micas commonly have a strong preferred orientation. Although detrital micas locally have basal planes oblique to S_2, micas with large aspect ratios tend to be oriented with basal planes subparallel to S_2. Cleavage development was contemporaneous with the growth of chlorite, muscovite, and quartz fibers (Fi_2) in pressure shadows around framboidal pyrite (Fig. 4) and in fibrous beards at the boundaries of detrital grains.

In several samples (e.g. D-18, D-22 and D-12), siderite or chlorite porphyroblasts overgrew the minerals that defined S_2 at the completion of D_2 (Fig. 4). These porphyroblasts contain straight trails of opaque particles, inert quartz grains (S_i), and, more rarely, pyrite pressure shadows that record only D_2 overgrowths (Figs. 4d & e). The chlorite porphyroblasts commonly occur in proximity (<100 m) to 60 Ma old plutons. Although the majority of porphyroblasts are nearly circular, some have aspect ratios as large as 2:1, and the long axes of these porphyroblasts have variable orientations. An exception to this observation occurs in sample D-22, where siderite has locally nucleated along S_2-perpendicular cracks in the matrix. The aspect ratios of these porphyroblasts can be as large as 20:1 (Fig. 4f). These replacement veins overgrew the material adjacent to the cracks rather than filling open gaps. All porphyroblasts have straight inclusion trails, regardless of orientation or shape (i.e. aspect ratio), indicating that porphyroblast growth was static or did not accompany an appreciable amount of strain.

D_3 deformation resulted in an apparent clockwise rotation relative to S_2 (when viewed to the southwest). The difference in orientation between inclusion trails (S_i) and S_2 can be as large as 70° (sample D-18). The variability in the amount of rotation within individual samples is largely a function of variability in the initial orientation of the porphyroblast relative to S_2. Following the suggestions of Powell & Treagus (1970), many sections in different orientations were observed to ensure that the porphyroblasts were viewed in a plane that is perpendicular to the axis of rotation. The initial orientation of the porphyroblasts relative to S_2 was established by determining the orientation of the foliation inside the porphyroblast (S_i) relative to the long axis of the porphyroblast. The amount of apparent rotation was then measured for porphyroblasts that were circular, initially elongate perpendicular to S_2, and initially elongate parallel to S_2 (Fig. 5). In all four samples analyzed, porphyroblasts that were initially elongate parallel to S_2 record the smallest observed apparent rotations, circular porphyroblasts record intermediate rotations, and initially S_2-perpendicular porphyroblasts record the greatest apparent rotations. The deformation that produced these apparent rotations can be subdivided into two stages.

Stage 1 can only be observed in three samples with siderite porphyroblasts. During stage 1, coarse-grained (3–5 μm thick) siderite fibers grew at the margins of many of the siderite porphyroblasts (Fig. 6c). The siderite that composes these fibers is cleaner than the adjacent siderite porphyroblast, and the fibers are optically continuous with the porphyroblasts, indicating that fiber growth was syntaxial (i.e. the most recent fiber growth is at the tips of the fibers). The siderite fibers are consistently curved, with the earliest increments of stage 1 siderite growth rotated clockwise relative to the latest (as viewed to the southwest). Because the fibers and the siderite host have a single optical orientation, the curvature of fibers cannot be due to bending and must be a response to changes in the orientation of incremental extension relative to the porphyroblast during stage 1. Optical continuity also suggests that the porphyroblasts and stage 1 fibers behaved rigidly during both stage 1 and subsequent strain accumulations. Stage 1 fibers postdate development of the cleavage included within porphyroblasts, but the importance of stage 1 strain for both the further modification of this cleavage and the development of S_3 is not clear.

Stage 2 is characterized by the growth of straight, antitaxial fibers of chlorite, muscovite and quartz in pyrite pressure shadows, fibrous beards on detrital grains, and large fibrous beards at the margins of porphyroblasts (Figs. 4a & c). Some siderite porphyroblasts in sample D-18 have long straight fiber segments at the tips of the pressure shadow (i.e. latest growth) that may be contemporaneous with D_3. Stage 2 deformation may have modified the cleavage that formed during D_2, and, in only a few samples (e.g. 43-83, 18-84, D-22 and D-18), developed either a second cleavage (S_3) or an incipient crenulation cleavage. In sample D-18, S_3 selvedges are short, discontinuous and only observed at the margins of the siderite porphyroblasts. In this case, the presence of a second cleavage was a consequence of strain heterogeneity near the rigid porphyroblasts. Although the slaty cleavage may have rotated or strengthened in intensity during D_3, this cleavage is referred to as S_2 after the deformation event (D_2) when it initially developed.

The incremental strain histories for D_2 and D_3 within the landward belt and seaward belt are recorded by the syntectonic fibers in pressure shadows around framboidal pyrite and at the margins of siderite porphyroblasts. The growth direction for fibers must be determined before the incremental strain history can be calculated. Fiber growth in pyrite pressure shadows is typically treated as antitaxial (Durney & Ramsay 1973), with the oldest fiber increments at the fiber tips and the youngest fiber increments at the surface of the pyrite host. This is consistent with the observation that, in the few samples with a second cleavage (S_3) that cross-cuts S_2, the segments of the fibers which record extension in the plane of the later cleavage (Fi_3) are located closest to the pyrite host. In contrast, detrital grains show the opposite relationship, with the S_3-parallel fiber segments at the tips of the fibrous beards. Thus, syntectonic fiber growth at the margins of detrital grains is syntaxial, with fiber growth occurring 'outwards', from the detrital grain towards the adjacent matrix. In this study, only syntectonic fibers around spherical pyrite and siderite hosts were used for quantitative analysis.

Strain histories were calculated in cleavage-perpendicular thin sections using the Durney & Ramsay method (1973), which assumes that fiber growth occurs parallel to the incremental extension direction and that fiber segments behave rigidly during subsequent strain accumulations. This method also assumes that the axis of incremental extension for all strain increments is parallel to the plane of observation (i.e. in these examples, the thin section defines the XZ plane). In nearly all samples from the landward belt of the Kodiak Formation, pressure shadows observed in cleavage-parallel sections have roughly straight fibers, so fiber curvature is largely restricted to cleavage-perpendicular sections. In addition, strain histories calculated from opposing pressure shadows on a single pyrite framboid give nearly identical results, suggesting that the curved fibers are not sectioned obliquely.

The strain histories for 23 samples are depicted by three different graphs: (1) the cumulative incremental strain history ($\xi - \varepsilon$); (2) the orientation history ($\Phi - \varepsilon$); and (3) the progressive finite strain history (Θ − E) (Figs. 6 and 7). Cumulative incremental strain histories display changes in the incremental extension direction as strain accumulates. A horizontal path on this diagram represents a sharp bend in a fiber or a rigid rotation, whereas a vertical path represents straight fibers or coaxial extension. In these cumulative incremental strain diagrams, the orientation of strain increments is recorded relative to an arbitrary S_2-fixed reference frame and thus these diagrams differ from an orientation history ($\Phi - \varepsilon$) diagram where the orientation of cleavage relative to ε_3 (Φ) is recorded at each particular point in the overall strain history.

A $\Phi - \varepsilon$ diagram can be constructed from the cumulative incremental strain diagram, however, by making assumptions about the strain path and the response of the cleavage to accumulations of strain. In this study, I will assume that (1) the cleavage behaves as a passive line marker and (2) the strain history involves coaxial pure shear, with variations in ξ that correspond to rigid rotation of the rocks relative to the fixed extension direction. The final cleavage orientation Φ_n and cumulative strain value ε_n are the same as the final point on a $\xi - \varepsilon$ diagram. The cleavage orientation at the completion of the n − 1th increment is obtained by restoring the passive line rotation that occurred during the final strain increment and the rigid rotation between the final two increments. For example, the passive rotation can be obtained using the equation:

$$\tan \theta_n = (S_1 S_3) \tan \Phi_n, \qquad (1)$$

where Φ_n is the orientation of the passive line marker (i.e. cleavage) at the completion of the nth increment, S_1/S_3 is the ratio of principal stretches associated with the nth increment (note that S_3 cannot be obtained from syntectonic fibers and an assumption must be made about volume change, ΔV. In this case I assume $\Delta V = 0$ and $S_3 = 1/S_1$), and θ_n is the orientation of cleavage prior to the nth increment (before taking into account the rigid rotation between the nth and $n - 1$th increments). The rigid rotation between the nth and $n - 1$th increments is given by the cumulative incremental strain history as:

$$R_n = \xi_n - \xi_{n-1}, \qquad (2)$$

where ξ_n is the orientation of the nth fiber segment (i.e. orientation of incremental extension) and ξ_{n-1} is the orientation of the $n - 1$th fiber segment. The orientation of the cleavage at the completion of the $n - 1$th increment (Φ_{n-1}) is:

$$\Phi_{n-1} = \theta_n - R_n. \qquad (3)$$

This result can then be used in equations (1), (2) and (3) to determine the orientation of cleavage at the completion of the $n - 2$th increment. After reconstructing the orientation of the cleavage before each increment, the resulting $\Phi - \varepsilon$ diagram shows the orientation history of a passive marker that ended the history with a final orientation parallel to the cleavage.

In the special case where Φ_n is not equal to 0° and $R_n = \Phi_n - \theta_n$ (i.e. the rigid rotation is equal to the passive rotation), the cleavage (i.e. a passive line marker), does not change orientation relative to the incremental extension direction. If Φ_n is not equal to 0° and $R_n = 0$ (i.e. coaxial extension oblique to the cleavage), then $\Phi_n < \Phi_{n-1}$ (the cleavage was initially more oblique relative to the incremental extension direction prior to the nth increment of strain). Thus, coaxial strain causes progressive rotation of the cleavage into parallelism with the incremental extension direction, and a $\Phi - \varepsilon$ diagram reflects this rotation.

The progressive finite strain diagrams (Θ − E) in Figs. 6 and 7 show variations in the orientation of the principal axis of finite extension as a function of the magnitude of the principal stretch. These diagrams can be used to consider the finite strain state at intermediate stages in the strain history as well as to compare the orientations of the cleavage and the axis of finite extension at the completion of the strain history.

Cumulative incremental strain histories, orientation histories, and progressive finite strain histories were determined for samples collected from coastline exposures along two across strike transects across the Kodiak Formation; the northeast coast of Afognak Island, and between Kodiak and Afognak Islands (Figs. 3, 6 and 7). In all samples, the cumulative incremental strain history involves an early, roughly coaxial strain

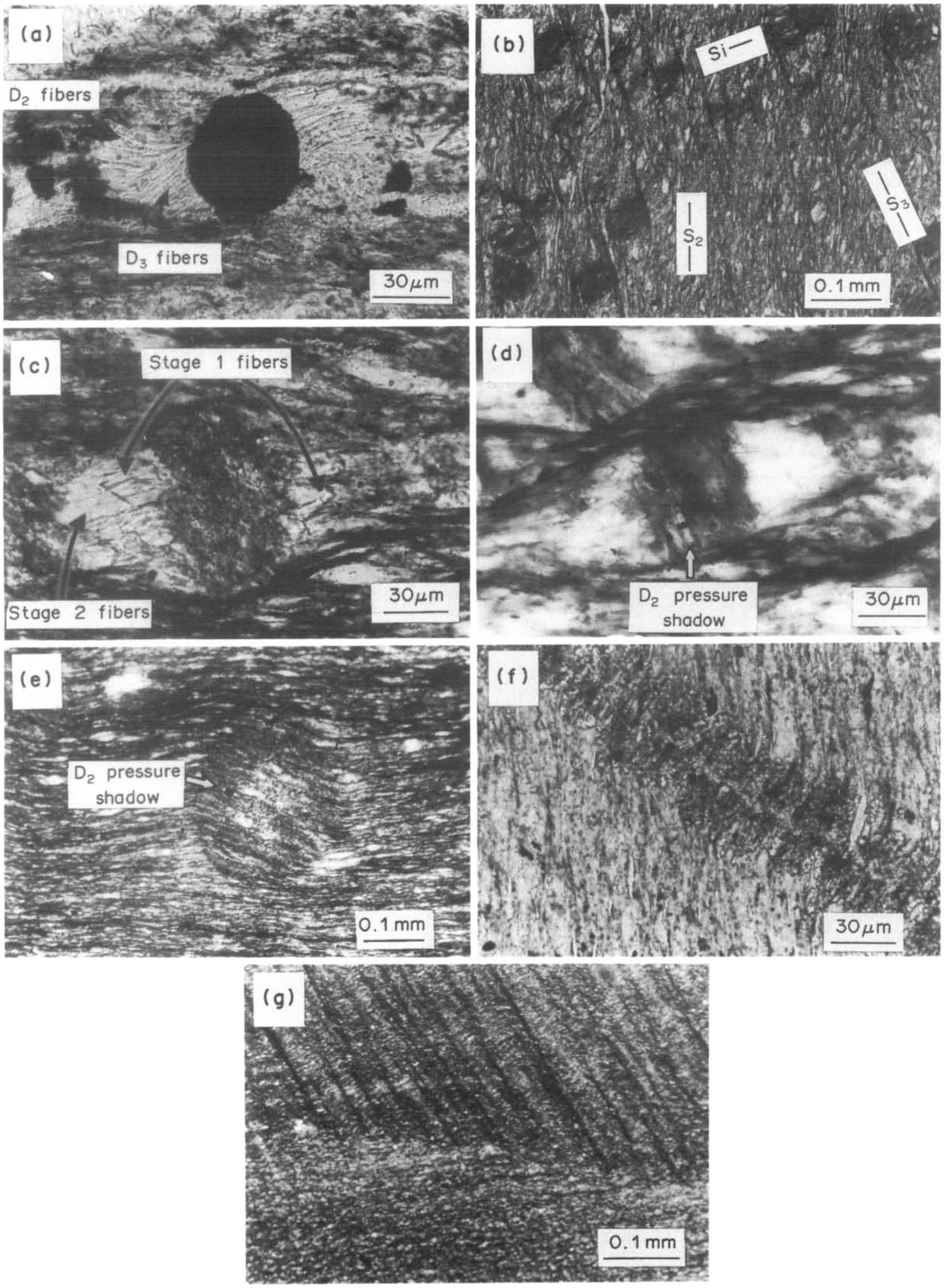

Fig. 4. Photomicrographs from sample D-18 in landward belt (except where noted). (a) Pyrite pressure shadow with D_2 and D_3 fiber growths. (b) Siderite porphyroblasts. S_2, S_i (traces of S_2 preserved in porphyroblasts) and S_3. Note that S_3 is restricted to margins of porphyroblasts. (c) & (d) Siderite and (e) chlorite (sample 38-84) porphyroblasts. Note fibrous overgrowths on siderite in (c). Curved coarse stage 1 siderite fibers occur closest to porphyroblast (darker overgrowth) with later straight stage 2 chlorite fibers (light overgrowth) at outer portion of pressure shadow. S_2 is horizontal and S_3 dips 20–30° to left. In (d) & (e) porphyroblast overgrows a pressure shadow that only records D_2 coaxial deformation parallel to S_1. (f) Siderite porphyroblast or replacement vein that nucleated along cracks in matrix. Traces of S_2 are preserved within porphyroblast and indicate that cracks were initially perpendicular to S_2. (g) Crenulation cleavage in sample 39-84 that is well developed where slaty anisotropy is strong (top) and absent in adjacent siltier layer (bottom) where slaty cleavage is weaker. In upper layer, D_2 strain resulted in development of parabolic yield curve in $\Phi - \sigma$ space and unstable behavior during subsequent strain, whereas in lower layer, D_2 strain was insufficient to produce a parabolic yield curve and later deformation was stable and homogeneous. All plane light except (d) with nicols crossed.

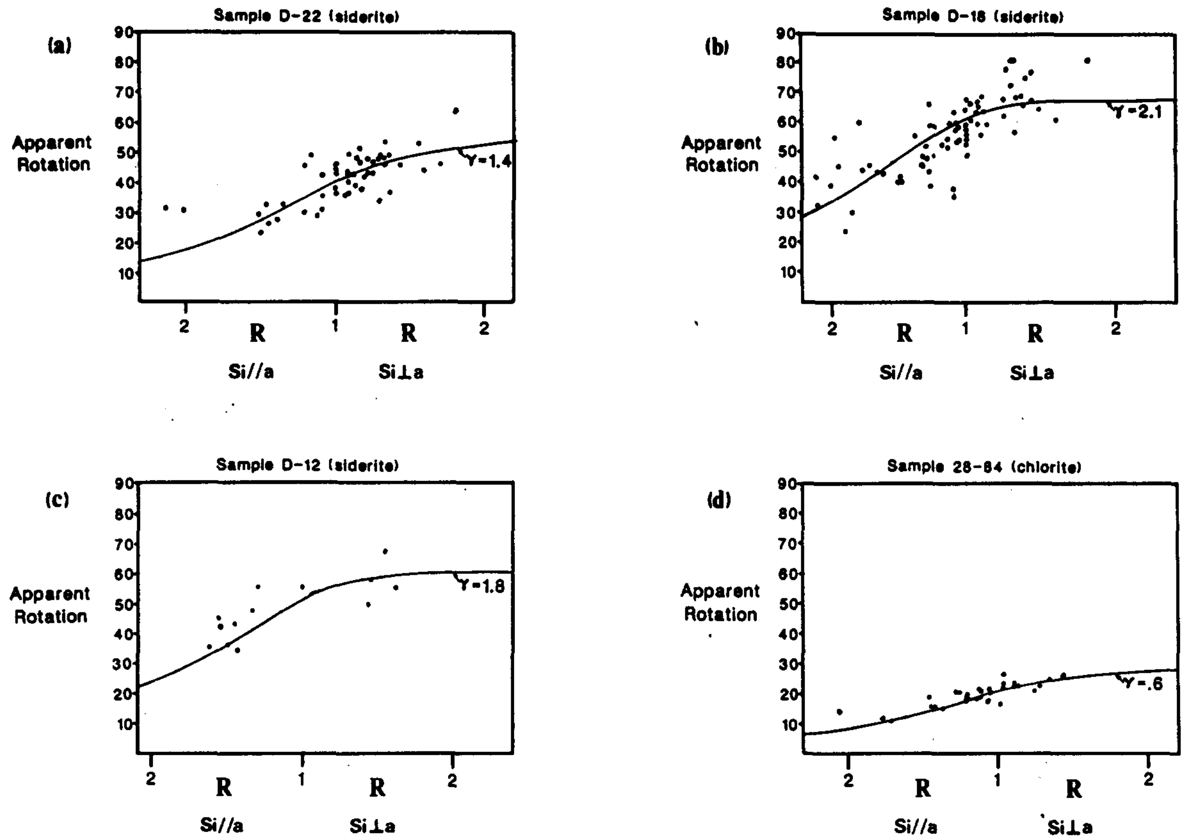

Fig. 5. Plot showing on y axis the differences in orientation between S_2 and S_i (i.e. apparent rotation in degrees) for porphyroblasts with different aspect ratios ($R = a/b$, where a and b are long and short axes, respectively, of cross-sectional ellipse). Apparent rotation was only measured for porphyroblasts which were originally elongate parallel to S_2 ($S_i \parallel a$), originally elongate perpendicular to S_2 ($S_i \perp a$), and circular ($R = 1$). Solid curves are calculated using the theoretical predictions of Ghosh & Ramberg (1976) for viscous flow around rigid elliptical inclusions, assuming progressive simple shear, a cleavage-parallel shear plane, and various shear strains (γ). (a) Sample D-22, $\gamma = 1.4$, (b) sample D-18, $\gamma = 2.1$, (c) sample D-12, $\gamma = 1.8$, (d) sample 28-84, $\gamma = 0.6$.

accumulation (Fi_2), followed by a rigid rotation and a second, roughly coaxial strain accumulation (Fi_3). In the landward belt, the cumulative elongation (sum of elongations) for increments of D_2-related strain varies from 0.272 (sample D-26) to 1.45 (sample 24-84). The orientation of this coaxial strain accumulation relative to S_2 varies from 8° (samples 16-84 and 24-84) to 44° (sample D-27) clockwise (cw). D_2-related strain is followed by a counterclockwise (ccw) rotation of 20° (sample 16-84) to 75° (sample D-26) (viewed to the southwest). The rotation is associated with an elongation of less than 0.272 and can be treated as a rigid rotation. The second coaxial strain accumulation (D_3-related strain) involves a cumulative elongation of 0.136 (sample D-26) to 0.727 (sample 25-84), with variations in the orientation of incremental extension relative to S_2 from 2° (sample 17-83) to 47° (sample D-26) counterclockwise.

The primary difference between cumulative incremental strain histories in the seaward belt and the landward belt is that the rigid rotation between D_2- and D_3-related strain accumulations is clockwise rather than counterclockwise (Fig. 6). Cumulative elongations for the early coaxial strain event vary from 0.273 (sample TB-6) to 0.909 (sample TB-26), with variations in the orientation of incremental extension relative to S_2 from 10° (sample TB-6) to 35° (TB-26) counterclockwise (Fig. 9). This strain accumulation is followed by a clockwise rigid rotation of 19° (TB-6) to 35° (TB-26). Cumulative elongations for D_3-related strain vary from 0.182 (sample TB-6) to 0.591 (sample TB-26). The orientation of incremental extension relative to S_2 for this event varies from 7° (sample TB-6) to 35° (sample TB-26) clockwise. Thus, the cumulative strain histories in the seaward belt (i.e. all TB samples) are roughly a mirror image of the cumulative strain histories in the landward belt in that the seaward belt and landward belt histories display clockwise and counterclockwise rigid rotations, respectively. The regional significance of this result is discussed in Fisher & Byrne (in preparation).

In both the landward belt and seaward belt, the incremental strain history (excluding stage 2) is approximated by two coaxial strain accumulations (D_2 and D_3) separated by a rigid rotation. Stage 2 is not included in this strain history because there is no evidence for this strain in pyrite pressure shadows. An idealized $\xi - \varepsilon$ curve for the strain history from pyrite pressure shadows would involve a vertical segment ($\xi = \xi_2$ not equal to 0°) followed by a horizontal segment (where ξ changes sign or crosses the axis $\xi = 0°$) and finally a vertical segment ($\xi = \xi_3$ not equal to 0°) (Fig. 8). An idealized $\Phi - \varepsilon$ curve would begin with a vertical segment at $\Phi = 90°$ (D_2)

followed by a horizontal segment to $\Phi = ((90 - \xi_3)$ + the passive rotation incurred during $D_3)^\circ$ and finally a curved path with Φ decreasing to $\Phi = (90 - \xi_2)^\circ$ as the cleavage rotates towards perpendicular to the D_3 shortening direction. Systematic deviations of calculated $\Phi - \varepsilon$ curves from this idealized curve can be attributed to a failure in one of the assumptions such as passive cleavage behavior.

The calculated $\Phi - \varepsilon$ diagram traces the orientation history from the final increment of strain backwards through the strain history, and an error at some stage in the orientation history is compounded for all previous strain increments. For example, if the calculated orientation of Φ prior to the rigid rotation in the observed strain histories (orientation of Φ at the completion of D_2, or Φ_2) is not equal to 0°, then the D_2 coaxial strain accumulation will not remain vertical on a $\Phi - \varepsilon$ diagram (as in the idealized case) but will be represented by a curved path with Φ increasing to a final value of Φ_2. This $\Phi - \varepsilon$ path is not likely, because the cleavage should form parallel to the extension direction during an initial coaxial strain accumulation. I will disregard the $\Phi - \varepsilon$ path for the early increments of coaxial strain and concentrate on the value of Φ_2. The magnitude of the

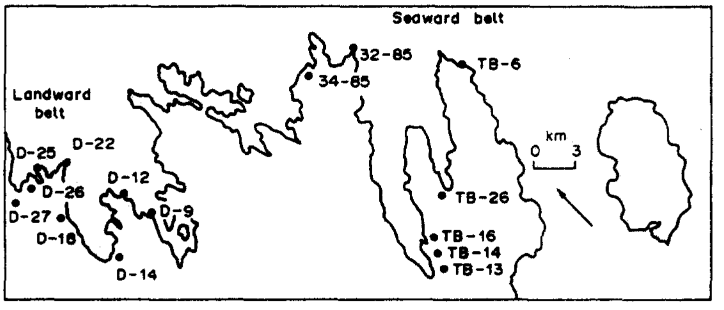

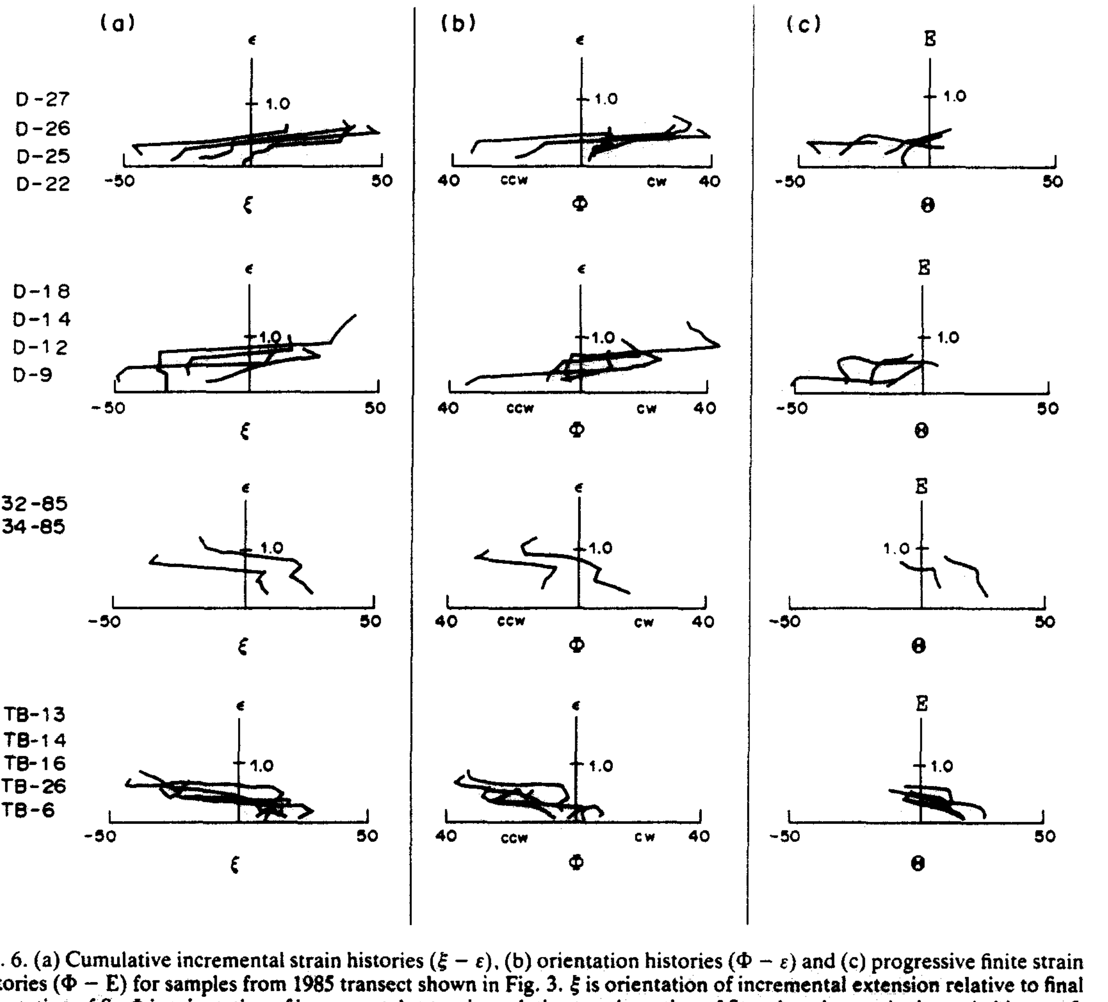

Fig. 6. (a) Cumulative incremental strain histories ($\xi - \varepsilon$), (b) orientation histories ($\Phi - \varepsilon$) and (c) progressive finite strain histories (Φ – E) for samples from 1985 transect shown in Fig. 3. ξ is orientation of incremental extension relative to final orientation of S_2. Φ is orientation of incremental extension relative to orientation of S_2 at that given point in strain history. Φ values are labelled cw and ccw depending on whether the shortening direction is measured clockwise or counterclockwise relative to S_2. Θ is orientation of finite extension relative to final orientation of S_2. ε is cumulative incremental elongation and E is progressive finite elongation. $\Phi - \varepsilon$ curves plot on left when shortening direction is measured clockwise relative to cleavage, and on right when shortening direction is measured counterclockwise. Histories are described in text.

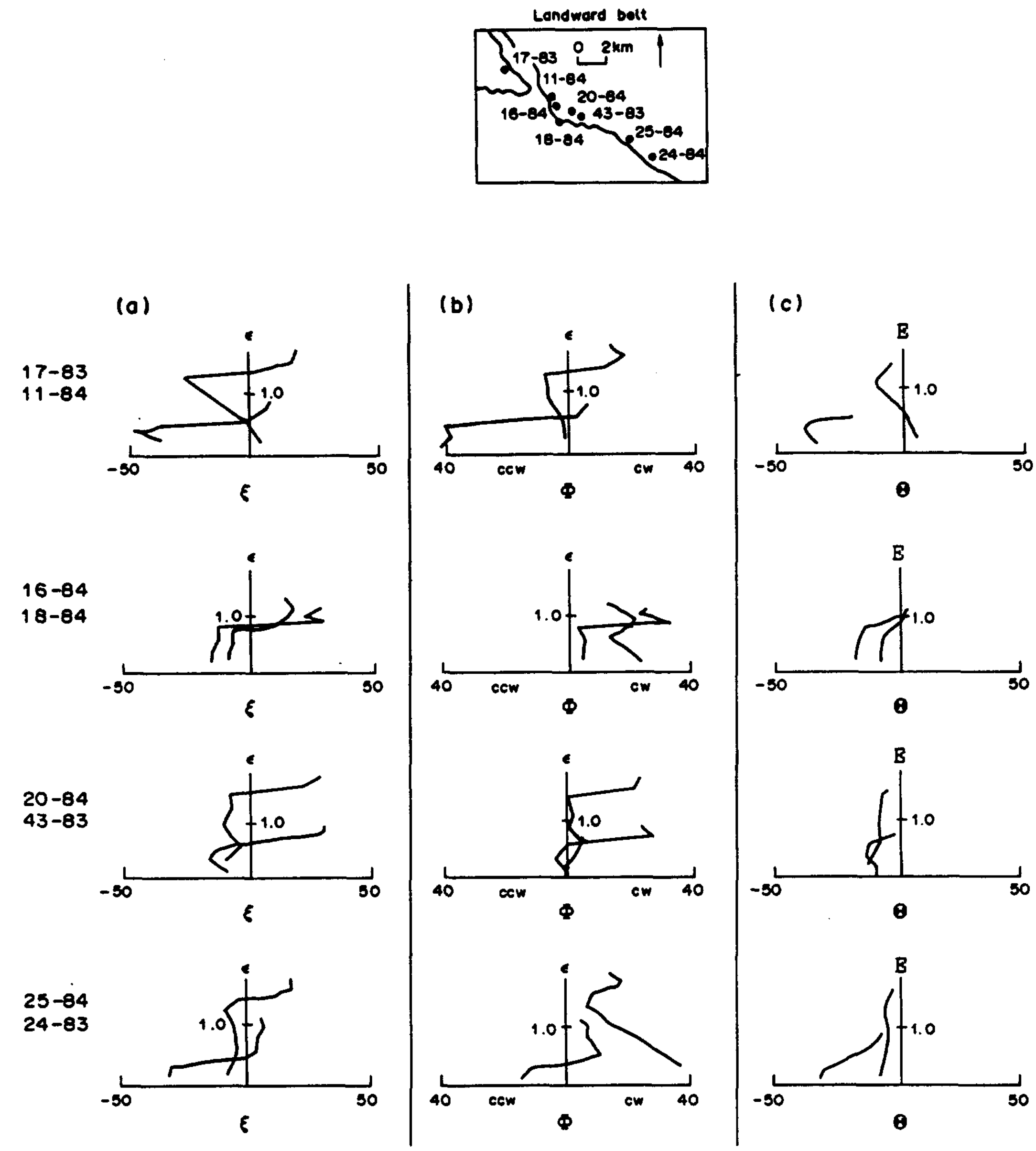

Fig. 7. (a) Cumulative incremental strain histories ($\xi - \varepsilon$), (b) orientation histories ($\Phi - \varepsilon$) and (c) progressive finite strain histories (Θ – E) for samples from 1983–1984 transect shown in Fig. 3.

deviation of this value from 0° is a measure of how reasonable the passive rotation assumption is for cleavage behavior during D_3 coaxial strain.

The value of Φ_2 for each measured strain history in the

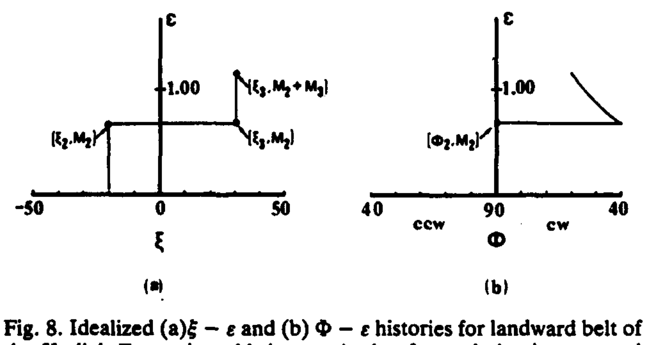

Fig. 8. Idealized (a)$\xi - \varepsilon$ and (b) $\Phi - \varepsilon$ histories for landward belt of the Kodiak Formation. M_2 is magnitude of cumulative incremental elongation at completion of D_2. M_3 is magnitude of cumulative incremental elongation associated with stage 2 of D_3. $M_2 + M_3$ is cumulative incremental elongation at completion of D_3.

landward belt and seaward belt was plotted as a function of: (1) the ratio of M_2 to M_3; (2) the magnitude of cumulative incremental extension during the first coaxial strain accumulation (M_2); and (3) the magnitude of cumulative extension during the second coaxial strain accumulation (M_3) (Fig. 9). Forty-two points were plotted on each graph because, wherever possible, several strain histories were determined for each of the twenty three samples. For $M_2/M_3 < 2$, there is a considerable amount of variability in the value of Φ_2, with values ranging from 42° ccw to 51° cw ($N = 23$, mean = 6° ccw, S.D. = 20°). For ratios of $M_2/M_3 > 2$, there is less scatter, with all values between 20° ccw and 20° cw ($N = 19$, mean = 1° cw, S.D. = 14°). A similar pattern is observed on plots of M_2 vs Φ_2, with variations in Φ_2 from 50° cw to 20° ccw at $M_2 < 0.5$ ($N = 19$, mean = 10° ccw, S.D. = 18°) and variations from 24° cw to 22° ccw for $M_2 > 0.5$ ($N = 23$, mean = 0°, S.D. = 14°). There is no apparent relationship between Φ_2 and M_3.

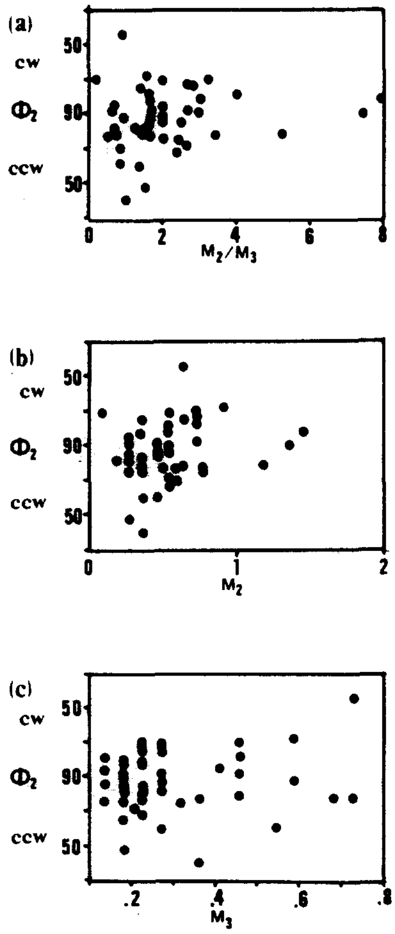

Fig. 9. Scatter diagrams showing (a) ratio of D_2 to D_3 elongation (M_2/M_3) vs Φ_2 (as defined in text), (b) M_2 vs Φ_2 and (c) M_3 vs Φ_2. Φ_2 is plotted as cw (clockwise) or ccw (counterclockwise), depending on orientation of shortening direction relative to reconstructed orientation of cleavage when viewed to southwest. For seaward belt, Φ_2 is plotted as viewed to northeast. M_2 and M_3 are same as in Fig. 8.

For samples with low values of M_2, the greater variability in Φ_2 may reflect variability in the local orientation of the weakly developed anastomosing cleavage rather than variations in mechanical behavior. Larger M_2 values result in a stronger early cleavage and a more uniform cleavage orientation at the scale of the pyrite strain markers. The mean values of Φ_2 for samples with low values of M_2 and M_2/M_3 are counterclockwise, suggesting that the cleavage rotates faster than a passive line marker when the fabric is poorly developed. Thus, for low values of M_2, the cleavage is weakly defined and easily modified into near parallelism with the extension direction during stage 2 of D_3 (e.g. samples 17–83 and 25-84). For larger values of M_2, the well developed cleavage behaves roughly as a passive line marker during subsequent strain accumulations.

The orientation of finite extension relative to the cleavage (final Θ value in the progressive finite strain history, Θ_f) can also be compared with values of M_2/M_3, M_2 and M_3 (Fig. 12). For $M_2/M_3 < 2$, Θ_f varies from $-22°$ to $+18°$ ($N = 25$, mean $= -2°$, S.D. $= 9°$), and, for $M_2/M_3 > 2$, Θ_f varies from $-11°$ to $+10°$ ($N = 19$, mean $= -2°$, S.D. $= 6°$). For $M_2 < 0.5$, Θ_f varies from $-22°$ to $+18°$ ($N = 20$, mean $= -2°$, S.D. $= 9°$) and, for $M_2 > 0.5$, Θ_f varies from $-11°$ to $+14°$ ($N = 24$, mean $= -2°$, S.D. $= 7°$). Thus, the orientation of the slaty cleavage becomes a better approximation to the orientation of finite extension as the magnitude of early coaxial strain (which led to initial development of the cleavage) becomes larger.

Only three of the samples analyzed (that do not have porphyroblasts) display an incipient crenulation cleavage, indicating that plastic deformation of the slaty groundmass of these samples occurred within the field of unstable slip or buckling (samples 18-84, 43-83 and D-22). These samples display a rigid rotation between the two coaxial strain accumulations of greater than 40°. M_2 values for the three samples range from 0.545 to 0.727. Seven other samples (samples 17-83, D-26, D-25, D-14, D-27, 9-83 and D-9) also record rigid rotations of greater than 40°. However, in contrast to the samples that developed a second cleavage, M_2 values for these samples are lower and range from 0.091 to 0.455. Thus, the occurrence of a crenulation cleavage depends on both the amount of rigid rotation and the amount of strain associated with cleavage development prior to the rigid rotation.

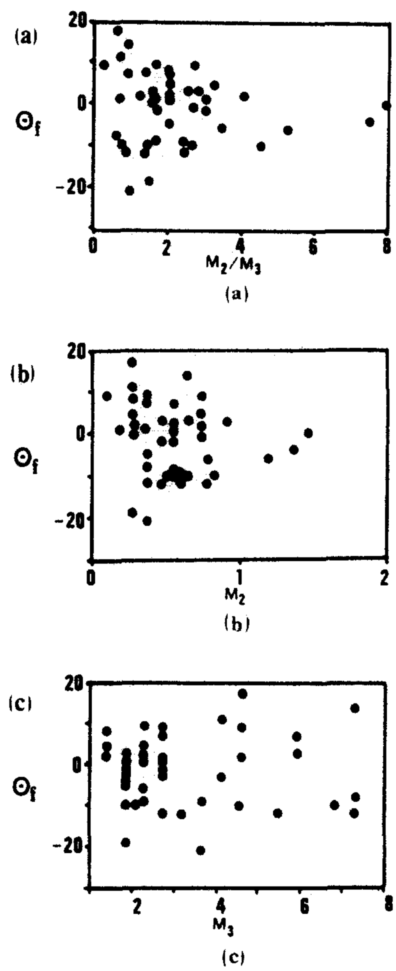

Fig. 10. Scatter diagrams showing (a) M_2/M_3 vs Θ_f, (b) M_2 vs Θ_f and (c) M_3 vs Θ_f. Θ_f is orientation of principal axis of finite extension at completion of D_2 and D_3. M_2 and M_3 are same as in Figs. 8 and 9.

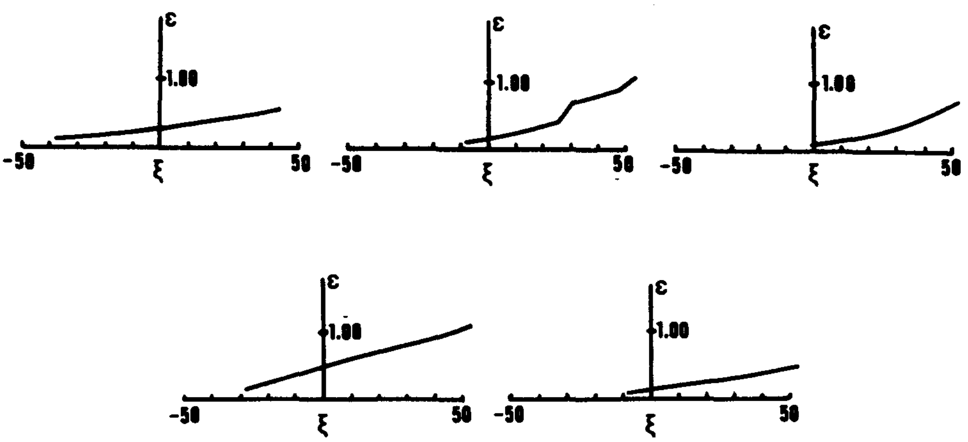

Fig. 11. Cumulative incremental strain histories for stage 1 of D_3 in sample D-18.

These analyses depend on the assumptions that there was no volume loss and that the strain path associated with D_2 and D_3 was coaxial pure shear. Fibers in pressure shadows record the orientation and magnitude of extension associated with each increment of deformation, but the strain ratio for each corresponding strain increment must be known before changes in volume can be quantified. Nevertheless, in other slates where large volume loss has been demonstrated such as the Martinsburg Formation and Hamburg Klippe in Pennsylvania (Wright & Platt 1982, Beutner & Charles 1985), fibrous overgrowths are absent or negligible (Beutner & Charles 1985, Wright personal communication). Moreover, a measurable volume loss during D_3 would cause cleavage to appear to rotate more than a passsive line marker on $\Phi - \varepsilon$ diagrams (which assume constant volume). This would skew Φ_2 towards counterclockwise (ccw) values, particularly for large values of M_3. Although the data in this case may be insufficient to make a definitive statement about volume loss, the Φ_2 values in Fig. 9(c) are roughly symmetric about $\Phi = 90°$ and large overgrowths are observed in pressure shadows around pyrites and detrital grains, so there was probably not an appreciable loss of volume. The assumption of pure shear is consistent with the observation that the cumulative incremental strain histories for D_2 and D_3 are roughly coaxial and do not commonly show consistent gradual rotations that could be associated with progressive simple shear.

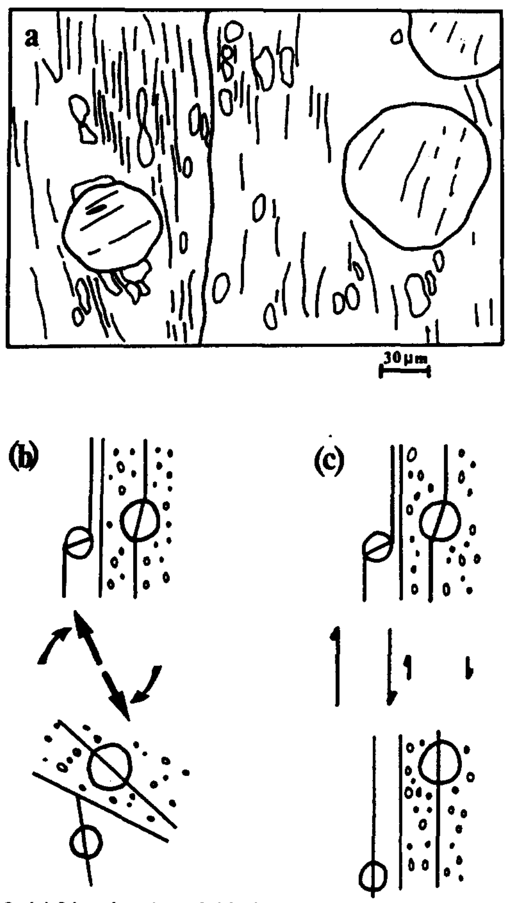

Fig. 12. (a) Line drawing of siderite porphyroblasts in silty (right) and pelitic (left) layers within sample D-18. Note that porphyroblasts are rotated more relative to bedding in pelitic layers. Also note that S_i is at high angles to bedding in pelitic layers and low angles to bedding in silty layers. (b) & (c) Two models which would produce stage 2 curved fibers and the relationship between bedding and S_i shown in (a). Gradual rigid rotation during (b) pure shear or (c) a component of simple shear.

Pyrite pressure shadows record only D_2 and stage 2 of D_3. In samples that contain siderite porphyroblasts (samples D-22, D-18 and D-12), syntaxial siderite fibers record penetrative strain accumulated during stage 1. In most cases these fibers are very short, given the amount of strain indicated by the apparent rotation of porphyroblasts. Cumulative incremental strain histories for stage 1 in sample D-18 are shown in Fig. 11. Sample D-18 is shown because, in the other two samples, the stage 1 fibers are too short to be suitable for incremental strain analysis. In sample D-18, the first increment of stage 1 strain (fiber segment closest to the siderite host) is oriented at between 0° and 38° cw in relation to the slaty cleavage. There is a gradual counterclockwise rotation of the extension direction (viewed to the southwest) and the final orientation of extension relative to the slaty cleavage is between 55° and 42°. The total amount of rotation varies from 50° to 80°, the final value of the cumulative incremental strain varies from 0.545 to 1.09, and the gradient $d(\xi)/d(\varepsilon)$ varies from 6.9°/0.1 to 14.7°/0.1. The gradient associated with this non-coaxial strain accumulation is steeper than gradient expected for progressive simple shear (5.7°/0.1, Gray & Durney

1979). Nevertheless, the siderite fibers may not reflect the strain in the surrounding matrix because stage 1 fiber growth rate is controlled by the dissolution, diffusion, or precipitation of siderite rather than matrix minerals.

Porphyroblasts of all shapes and initial orientations display stage 1 fibers with a gradual counterclockwise rotation. Thus, the apparent rotation of porphyroblasts cannot be solely the result of passive rotation of cleavage with respect to nonrotating porphyroblasts (i.e. coaxial pure shear model; Ramsay 1962, Bell *et al.* 1986). Although some of the apparent rotation of porphyroblasts may be accounted for by passive rotation of S_2 relative to the porphyroblasts during stage 2 coaxial deformation, stage 1 fibers indicate non-coaxial strain that may also have resulted in apparent rotation of porphyroblasts by either: (1) passive rotation of cleavage during gradual clockwise rigid rotation of the rock body through a fixed extension direction (Beutner & Diegel 1985, Sample & Fisher 1986) or (2) rotation of porphyroblasts in response to a component of progressive simple shear.

A comparison of porphyroblasts in competent (siltstone) and incompetent (shale) lithologies supports model 2. In both siltstone and shale layers, the slaty cleavage is nearly parallel to bedding. The foliation preserved within porphyroblasts (S_i) is rotated 40–75° cw relative to the slaty cleavage in shale layers, yet only 10–30° in siltstone layers (Fig. 12). This result could be accounted for with either of the two models if there was less penetrative strain in competent layers where the cleavage is only weakly developed. However, if apparent porphyroblast rotation were a response to rigid rotation of the rock body during coaxial deformation, then silt layers (which were only weakly deformed), spherical porphyroblasts in shale layers (which were rigid), and porphyroblasts in silt layers (also rigid) would have experienced a rigid rotation of similar magnitude. The orientation of S_i relative to bedding for spherical porphyroblasts should not have changed significantly after D_2 and should represent the orientation of the cleavage relative to bedding prior to D_3. In silt layers, S_i is oriented at a low angle to bedding whereas in shale layers, S_i is at a high angle to bedding. Thus, the rigid rotation model requires the unlikely premise that cleavage initially refracted from a low angle relative to bedding in competent layers to a high angle to bedding in incompetent layers.

Alternatively, the progressive simple shear model requires only that shear strain on planes subparallel to bedding is greatest in the least competent units. The present orientation of S_i relative to bedding would not be the same as existed after D_2 because, during stage 1, there was active rotation of porphyroblasts in response to a component of simple shear. The final orientation of extension recorded by stage 1 fibers relative to the slaty cleavage (40–50°) and the amount of rotation recorded by porphyroblasts of various shapes and initial orientations (Fig. 8) are consistent with a shear plane nearly parallel to the cleavage. The amount of porphyroblast rotation indicated by stage 1 fibers suggests that the simple shear strain (γ) for stage 1 in sample D-18 was approximately 2. In the absence of stage 1 fibers, it is impossible to determine if any simple shear was involved, and apparent rotation could be explained by passive rotation of the cleavage relative to the porphyroblasts during stage 2 coaxial strain.

CONCLUSIONS

The total strain history for D_2 and D_3 involved a coaxial strain accumulation (D_2) with shortening perpendicular to cleavage ($\Phi \cong 90°$) followed by a non-coaxial strain accumulation due to a component of progressive simple shear with a cleavage at a high angle ($\Phi \cong 45°$) to the shortening direction (event 2) and finally, a second coaxial strain accumulation with cleavage oblique relative to the shortening direction ($\Phi \cong 20$–40°). These penetrative strains coincide with structural events which are recognized in the field based on mesoscopic and map scale structures (Fisher & Byrne in preparation).

Stage 1 of D_3 is only recognized in samples that have porphyroblasts. Apparently there was little fiber growth in pyrite pressure shadows during the initial rotation of porphyroblasts. Stage 1 deformation may have been dominated by plastic processes such as dislocation creep or independent particulate flow rather than by a redistribution of mass by diffusive mass transfer. There are several possible explanations for variations in the dominant deformation mechanism. An increase in bulk strain rate would result in an increase in the relative importance of plastic processes, but the absolute strain rate contribution of diffusive mass transfer should remain constant. Alternatively, for a constant bulk strain rate, an increase in temperature could lower the yield stress associated with basal-slip in micas, and the strain rate contribution of diffusive mass transfer would decrease. Finally, for a constant temperature and bulk strain rate, the strain rate contribution of diffusive mass transfer could have decreased as a consequence of the orientation history. During stage 1, Φ was close to 45° and the yield stress for plastic processes may have been negligible or at least lower than for D_2 and stage 2 of D_3. Thus, variations in the relative importance of diffusive mass transfer and plastic processes may coincide with variations in deviatoric stress that are controlled by the orientation history.

Inferences about the relationship between deviatoric stress and orientation history depend on the assumption that, throughout the strain history, the deviatoric stress was on the parabolic yield curve for plastic processes. In the field of stable slip, this assumption is difficult to test because there is little textural record for plastic deformation in slates. In the field of unstable slip, plastic deformation is recorded by buckling instabilities within the rock matrix. Buckling is observed in several samples where the rigid rotation from D_2 to D_3 was greater than 40°. However, the yield stress for plastic processes may be low in these cases (i.e. close to the lowest points on the parabola). In the central belt of the Kodiak Formation (strain histories for this region are discussed in Fisher & Byrne in preparation), a crenulation cleavage occurs nearly orthogonal to the slaty cleavage. Moreover, in the landward belt, a sample from the hinge of a rare small-scale D_3 fold (sample D-17 located within 10 m of sample D-18) has a crenulation cleavage (S_3) orthogonal to S_2. The deviatoric stress must be on the yield curve for plastic deformation in these cases where Φ is close to 0°. Thus, for rocks with a strong mechanical anisotropy, the stress–strain history can be inferred from the orientation history recorded by incremental strain markers. In the landward belt, the region would have experienced strain hardening during D_2 followed by deformation at a lower stress at the onset of D_3, and finally, strain hardening during stage 2 of D_3.

Given that plastic processes are always operative, there are two factors that determine whether a second cleavage will be present after a strain history involving two coaxial strain events separated by a rigid rotation: (1) the amount of strain associated with cleavage development and (2) the orientation history. When strain associated with D_2 was small, the slaty cleavage was only weakly developed, and a crenulation cleavage did not form, even after a rigid rotation of greater than 45°. This observation suggests that a parabolic yield curve for plastic deformation develops only after the strain has succeeded in aligning mica grain boundaries and basal planes into a mechanically significant anisotropy. In the case where D_2 strain is not sufficient to establish a parabolic yield curve, a rigid rotation followed by a second strain event will either unstrain the pre-existing fabric or cause the development of a diffuse or pervasive fabric that cuts the earlier fabric (Fig. 6g). In either case, a spaced crenulation cleavage will not develop.

The other factor which controls crenulation cleavage development is the orientation history. In the Kodiak Formation and in samples described by Gray & Durney (1979), crenulation cleavages only formed in samples when the rigid rotation was greater than 45°, indicating that the field of unstable sliding (once a parabolic yield curve is established) encompasses Φ values of 0° to 45°. This suggests that the angle of internal friction (Ψ) is close to 0°, and thus, dislocation creep with slip on basal planes of micas may be more important than frictional sliding on grain boundaries in these low-grade rocks.

An arbitrary strain history will only reach the field of unstable sliding if a $\xi - \varepsilon$ history has an episode where the gradient $d\varepsilon/d\xi$ is small (i.e. the rigid rotation is greater than the passive rotation of opposite sense). This occurrence can be recognized by constructing a $\Phi - \varepsilon$ plot using the data from the $\xi - \varepsilon$ history. If Φ is constant or approaches 90°, then deformation is stable. If Φ approaches 0° then a crenulation cleavage will develop when the orientation history enters the field of unstable sliding.

Acknowledgements—Logistical support was provided in the field by USGS, USCG, the Randalls, the Stovers and the Fields. This research was supported by a GSA Harold T. Stearns Fellowship Award to the author, and NSF Grants EAR 8407801 and EAR 8306578. An earlier draft of the manuscript was improved as a result of critical reviews by Win Means, Jan Tullis, Terry Tullis, Tim Byrne, Jean Crespi, Steve Lucas, Bill Clendenen, Ed Beutner, Brian Bayly and two anonymous reviewers.

REFERENCES

Bell, T. H., Rubenach, M. J. & Fleming, P. D. 1986. Porphyroblast nucleation, growth and dissolution in regional metamorphic rocks as a function of deformation partitioning during foliation development. *J. metamorph. Geol.* **4**, 37–67.

Berner, R. A. 1978. Rate control of mineral dissolution under earth surface conditions. *Am. J. Sci.* **278**, 1235–1252.

Beutner, E. C. & Charles, E. G. 1985. Large volume loss during cleavage formation, Hamburg sequence, Pennsylvania. *Geology* **13**, 803–898.

Beutner, E. C. & Diegel, F. A. 1985. Determination of fold kinematics from syntectonic fibers in pressure shadows, Martinsburg slate, N.J. *Am. J. Sci.* **285**, 16–50.

Beutner, E. C., Fisher, D. M. & Kirkpatrick, J. 1988. Kinematics of deformation at a thrust fault ramp (?) from syntectonic fibers in pressure shadows. In: *Geometry and Mechanisms of Thrusting with Special Reference to the Appalachians* (edited by Mitra, C. & Wojtal, S.). *Spec. Pap. geol. Soc. Am.* **222**, 77–88.

Borradaile, G. J. 1979. Strain study in the Caledonides in the Islay region, SW Scotland: implications for strain histories and deformation mechanisms in greenschists. *J. geol. Soc. Lond.* **136**, 77–88.

Borradaile, G. J. 1981. Particulate flow of rock and the formation of cleavage. *Tectonophysics* **72**, 305–321.

Butler, R. W. H. 1982. Hangingwall strain: a function of duplex shape and footwall topography. *Tectonophysics* **88**, 235–246.

Byrne, T. & Fisher, D. M. 1987. Episodic growth of the Kodiak convergent margin. *Nature* **325**, 338–341.

Cobbold, P. R. 1977. Description and origin of banded deformation structures—II. Rheology and the growth of banded perturbations. *Can. J. Earth Sci.* **13**, 2510–2523.

Donath, F. A. 1961. Experimental study of shear failure in anisotropic rocks. *Bull. geol. Soc. Am.* **72**, 985–990.

Donath, F. A. 1964. Strength and deformation behavior in anisotropic rocks. In: *State of the Earth's Crust* (edited by Judd, W. R.). Elsevier, New York, 281–297.

Donath, F. A. 1968. Experimental study of kink-band development in Martinsburg slate. In: *Proc. Conference on Research in Tectonics* (edited by Baer, A. J. & Norris, D. K.). *Geol. Surv. Pap. Can.* **68-52**, 255–293.

Durney, D. W. & Ramsay, J. G. 1973. Incremental strains measured by syntectonic crystal growths. In: *Gravity and Tectonics* (edited by Dejong, K. A. & Scholten, R.). John Wiley and Sons, New York, 67–96.

Elliott, D. 1972. Deformation paths in structural geology. *Bull. geol. Soc. Am.* **83**, 2621–2638.

Elliott, D. 1973. Diffusion flow laws in metamorphic rocks. *Bull geol. Soc. Am.* **84**, 2645–2664.

Ellis, M. 1986. The determination of progressive deformation histories from antitaxial syntectonic crystal fibers. *J. Struct. Geol.* **8**, 701–709.

Etchecopar, A. & Malavieille, J. 1987. Computer models of pressure shadows: a method for strain measurement and shear-sense determination. *J. Struct. Geol.* **9**, 667–677.

Etheridge, M. A., Wall, V. J. & Vernon, R. H. 1983. The role of the fluid phase during regional metamorphism and deformation. *J. metamorph. Geol.* **1**, 205–226.

Fisher, D. & Byrne, T. 1987. Structural evolution of underthrusted sediments. *Tectonics* **6**, 775–793.

Ghosh, S. K. & Ramberg, H. 1976. Reorientation of inclusions by combination of pure shear and simple shear. *Tectonophysics* **34**, 1–70.

Gray, D. R. & Durney, D. W. 1979. Investigations on the mechanical significance of crenulation cleavage. *Tectonophysics* **58**, 35–79.

Kennan, P. A. 1971. Porphyroblast rotation and the kinematic analysis of a small fold. *Geol. Mag.* **108**, 221–228.

Kronenberg, A. K., Pinkston, J. C. & Kirby, S. H. 1985. Basal slip of biotite single crystals. *Eos* **66**, 366.

Lifshitz, I. M. 1963. On the theory of diffusion—viscous flow of poycrystalline bodies. *Soviet Physics, JETP* **17**, 909–920.

Moore, J. C., Byrne, T., Reid, M., Gibbons, H., Plumley, P. & Coe, R. 1983. Paleogene evolution of the Kodiak Islands, Alaska: conse-

quences of ridge–trench interaction in a more southerly latitude. *Tectonophysics* **2**, 265–293.
Patterson, M. S. & Weiss, L. E. 1966. Experimental deformation and folding of phyllite. *Bull. Geol. Soc. Am.* **77**, 343–374.
Powell, D. & Treagus, J. E. 1970. Rotational fabrics in metamorphic minerals. *Mineralog. Mag.* **37**, 801–814.
Ramsay, J. G. 1962. The geometry and mechanics of formation of 'similar' type folds. *J. Geol.* **70**, 309–327.
Ramsay, J. G. 1967. *Folding and Fracturing in Rocks*. McGraw-Hill, New York.
Ramsay, J. G. 1980. Shear zone geometry: a review. *J. Struct. Geol.* **2**, 83–100.
Ramsay, J. G. & Graham, R. H. 1970. Strain variations in shear belts. *Can. J. Earth Sci.* **7**, 786–813.
Ramsay, J. G. & Huber, M. I. 1983. *The Techniques of Modern Structural Geology, Volume* 1: *Strain Analysis*. Academic Press, New York.
Reches, Z. 1979. Deformation of a foliated medium. *Tectonophysics* **57**, 119–129.
Sample, J. & Fisher, D. 1986. Duplex accretion and underplating in an ancient accretionary complex, Kodiak Islands, Alaska. *Geology* **14**, 160–163.
Sample, J. & Moore, J. C. 1987. Structural style and kinematics of an underplated slate belt, Kodiak and adjacent islands, Alaska. *Bull. geol. Soc. Am.* **99**, 7–20.
Tapp, B. & Wickham, J. 1987. Relationships of rock cleavage fabrics to incremental and accumulated strain in the Conococheague Formation, U.S.A. *J. Struct. Geol.* **9**, 457–472.
White, S. H., Burrows, S. E., Carreras, J., Shaw, N. D. & Humphreys, F. J. 1980. On mylonites in ductile shear zones. *J. Struct. Geol.* **2**, 175–188.
Wickham, J. S. 1973. An estimate of strain increments in a naturally deformed carbonate rock. *Am. J. Sci.* **273**, 23–47.
Wickham, J. S. & Anthony, M. 1977. Strain paths and folding of carbonate rocks near Blue Ridge, central Appalachians. *Bull. geol. Soc. Am.* **88**, 920–924.
Williams, P. F. & Schoneveld, Chr. 1981. Garnet rotation and the development of axial plane crenulation cleavage. *Tectonophysics* **78**, 307–334.
Wright, T. O. & Platt, L. B. 1982. Pressure dissolution and cleavage in the Martinsburg shale. *Am. J. Sci.* **282**, 122–135.